AD-A055 905 CALIFORNIA UNIV BERKELEY DEPT OF CHEMICAL ENGINEERING F/G 11/9
STRAIN INDUCED PLASTIC-TO-RUBBER TRANSITION OF AN SBS BLOCK COP--ETC(U)
APR 78 J DIAMANT, M SHEN, T HASHIMOTO N00014-75-C-0955
UNCLASSIFIED TR-19 NL

END
DATE FILMED
8-78
DDC

(9) Technical Report No. 19

(12)

(6) Strain Induced Plastic-to-Rubber Transition of An SBS Block Copolymer and Its Blend with PS

By

T. Hashimoto, M. Fujimura, K. Saijo, and H. Kawai
Department of Polymer Chemistry
Faculty of Engineering
Kyoto University
Kyoto, Japan 606

and

(10) J. Diamant and M. Shen
Department of Chemical Engineering
University of California
Berkeley, California 94720

(14) TR-19

(11) 1 April 1978

(12) 36 P.

(15) N00014-75-C-0955

Technical Report to be published in

Advances in Chemistry Series

Approved for public release: Distribution Unlimited

Prepared for
Office of Naval Research
800 North Quincy Street
Arlington, Virginia 22217

Strain Induced Plastic-to-Rubber Transition of An SBS Block Copolymer and Its Blend with PS

By

T. Hashimoto, M. Fujimura, K. Saijo and H. Kawai
Department of Polymer Chemistry
Faculty of Engineering
Kyoto University
Kyoto, Japan 606

and

J. Diamant and M. Shen
Department of Chemical Engineering
University of California
Berkeley, California 94720

ABSTRACT

The strain softening phenomenon in poly(styrene-b-butadiene-b-styrene) and its blends with polystyrenes were investigated by means of electron microscopy and small angle x-ray scattering. Samples were cast from mixed solvents of tetrahydrofuran and methyl ethyl ketone (90/10 by volume). The structure of these samples consist of randomly oriented alternating lamellar domains of the two components. Their mechanical behavior is plastic-like in that they exhibit yielding and necking when first stretched to around 200%. After the necking has propagated throughout, the samples show typical rubber-like behavior. This phenomenon may be called the strain induced plastic-to-rubber transition, and is believed to occur as a result of structural changes from alternating lamellar domains to fragmented PS domains dispersed in a PB matrix. After the strain has been removed, the samples will spontaneously "heal" themselves, i.e., an inverse transition from rubber-like to plastic-like behavior will take place. The healing effect is also investigated by the same techniques. It was found that healing can occur by annealing at a temperature as low as 60°C

in a duration as short as 10 minutes. During the healing process, the original alternating lamellar structure is reformed. The effect was interpreted in terms of interfacial domain boundary relaxations activated with the fragmentation of the PS lamellar domains.

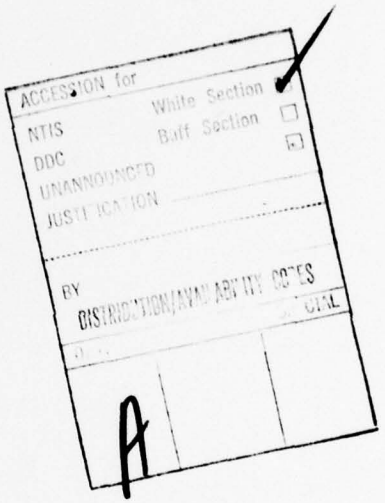

INTRODUCTION

It has been shown that some block copolymers and their blends with corresponding homopolymers exhibit the so-called strain softening effect. (1,2,3,4,5) When the plastic specimens are stretched beyond the yield point, it becomes rubbery and exhibits high-elasticity with large recoverable deformation due to the break-up of their original rigid structure. (1,6,7) Moreover, specimens after stretching exhibit a healing effect, in that properties of the original undeformed specimens are recovered upon removal of the applied stress. (1,4,5) The effect has been attributed to the reformation of the original microdomain structure. In this paper, the structural changes in a SBS block copolymer and its blends with homopolystyrene accompanying the strain-induced plastic-to-rubber transition and the healing process are investigated by means of electron microscopy and small angle X-ray scattering. The healing effect is rationalized in light of the domain-boundary relaxation mechanism.

EXPERIMENTAL

Research grade poly(styrene-b-butadiene-b-styrene), designated as TR-41-1647, TR-41-1648, and TR-41-1649, were received from Shell Development Co. These block copolymers contain 26.8, 29.3 and 48.2 wt% polystyrene (PS), respectively. The average molecular weights, determined by intrinsic viscosity measurements in toluene at 30°C, were found to be 7-36-6, 16-78-16, and 14-30-14 in units of thousands. The microstructures of polybutadiene (PB) blocks was found to contain about 40 mole% in cis 1,4, 50% in trans 1,4, and 10% in 1,2, units.

Film samples were prepared by spin-casting (6) from 10% solutions of the polymer in tetrahydrofuran and methyl ethyl ketone (90/10 by volume). Residual solvent was removed by heating in vacuo at 60°C until constant weight was reached. For electron microscope observations,

samples were stained by osmium tetraoxide and then cut normal to the film surface by an LKB ultramicrotome to a thickness of about 300 Å Samples that have been first stretched to 600% and then returned to the unstrained state were stained in aqueous solution of OsO_4 for 24 hr at room temperature and subsequently cut into ribbon shape, embedded in epoxy resin, trimmed, and stained again in the aqueous solution of OsO_4 for 5 to 12 hr at 50°C and then sectioned. To observe the morphology of samples in the stretched state, the specimens were first elongated to 85% and 500%, fixed into metal frames, and subsequently stained by OsO_4 vapor for 48 hr at room temperature under the stretched state. The stained specimens were then released from metal frames and treated in the manner described above for restaining and ultrathin sectioning. The fixation of the specimens by OsO_4 is more effective near the surfaces, therefore a partial contraction of the specimens occurs upon release from stretched state leading to a reduction of effective bulk strain to 64% and 200%, respectively.

To investigate the healing effect, the embedding process of the stained specimen into epoxy resin for trimming was not performed in order to avoid heat generation. In addition, temperature of the restaining process in aqueous solution of OsO_4 was reduced from 50°C to room temperature, thus eliminating extraneous heating in the healing process.

The SAXS patterns were obtained with nickel-filtered CuKα radiation at 40 KV and 100 mA using a rotaflex RU-100PL generator (Rigaku-Denki) and with a point focussing system so arranged that distances of the first and second pinholes, specimen, and photographic film from the focal spot are 128, 378, 438 and 738 mm, respectively. Sizes of the first and second pinholes are 0.5 and 0.2 mm in diameter. The SAXS intensity distributions were detected by a scintillation counter with a pulse-height analyzer. The same generator and the same power as in the photo-

graphic experiment were used as an incident X-ray source. The size of the focal spot was 0.5 x 5 mm^2 on target and 0.15 x 5 mm^2 in projection. The incident X-ray source was collimated using the following arrangement: the first, second and third slits, the specimen, and the counter and scattering slits were placed at 128, 378, 418, 443, 703 and 743 mm from the focal spot, respectively. The sizes of the first, second, counter, and scattering slits were 0.1 x 10, 0.1 x 10, 0.1 x 15, and 0.05 x 15 mm^2. The intensity distribution was measured by a conventional low angle X-ray goniometer (No. 2202, Rigaku-Denki) using a step scanning device with a step interval of 0.6 min, each for a fixed time of 100 sec. The measured scattered intensity distributions were corrected for collimation error by using the weighting function calculated from the Hendricks-Schmidt equations (7) using Schmidt's method of demearing (8), the detailed procedure of which has been described elsewhere. (9)

RESULTS AND DISCUSSION

Mechanical Properties

Figure 1 shows the cyclic tensile stress-strain behavior of the three block copolymer film specimens at 25°C at a constant rate of tensile strain of 50%/min. The tensile stress is expressed in terms of true stress, i.e., tensile force divided by actual cross-sectional area of the elongated specimen, and the tensile strain is expressed by extension ratio. The number of small arrows attached to the cyclic deformation curves indicate the first, second, and third stretch cycle. As can be seen in the figure, the yielding phenomenon becomes more pronounced with increasing styrene content (from TR-41-1647 to TR-41-1648 to TR-41-1649). The strain-softening effect resulting from the strain-induced plastic-to-rubber transition is particularly clear for the TR-41-1649 specimen. Presumably the randomly oriented styrene lamellae has been elastically deformed up to the yield-point, beyond which the lamellae disintegrate into fragments and dispersed

in the butadiene matrix to result in strain-softening.

Figure 2 shows again the tensile stress-strain behavior of TR-41-1649 and its PS blend measured in first and second stretches. The experiment was conducted at room temperature at a strain rate of 50%/min. For clarity only the stretching half-cycles are shown. Here the tensile stress is expressed in terms of nominal stress, i.e., tensile force divided by original cross-sectional area of the specimen, and the tensile strain is expressed as %-elongation. As can be seen in the first stretching half-cycle in the figure, after the yielding has taken place there is a plateau region followed by a rapid increase of the stress. These regions are more clearly discernable than those shown in Fig. 1 where true stress was used.

The block copolymer exhibits a yield point at around 5% strain, after which the stress decreases until about 20% strain. The stress then remains constant with further elongation up to about 180% strain. This is typical plastic-like behavior. When the applied stress exceeds the yield stress, necking suddenly appears at a localized region in the specimen, which subsequently grows continuously until the whole specimen is covered. The necking process gives rise to the plateau region observed in the stress-strain curve. Upon further stretching, the stress rises rapidly and fracture soon follows. If the deformation process is reversed, there is now substantial strain recovery. Thus the initially plastic-like specimen becomes rubber-like at the completion of the necking process. The stress-strain behavior during the second cyclic deformation is also rubber-like and does not show any yielding and necking phenomena except for a small but rapid increase in stress at the beginning of the second stretching half-cycle.

The blended specimen exhibits similar strain-induced plastic-to-rubber transition or the strain-softening, as clearly seen in Fig. 2.

Due to the higher overall PS content of the specimen it shows a higher value of Young's modulus (initial modulus), yield stress, stress at the plateau region, and the tangent modulus after completion of the necking. The observed residual strain after removal of the applied stress is also higher than the SBS specimen. It is interesting to note that the difference in stress-strain behavior of the block copolymer and the blend becomes less pronounced for the second stretch half cycle.

Electron Microscopy

Figure 3 shows electron micrographs of ultrathin sections of film specimens of the three kinds of block copolymers. As can be seen in the figure, TR-41-1647 and TR-41-1648 specimens have a heterogeneous structure in which the polystyrene domains are dispersed within a polybutadiene matrix and are connected to each other to form a swirl-like structure. On the other hand, TR-41-1649 specimen is seen to consist of alternating lamellar domains of the two components. Changes of the domain structure with fractional compositions of styrene and butadiene components are consistent with predictions of the current theories of micro-phase separation (9,10,11,12) for block copolymers cast from such a nearly nonselective solvent as the mixture of tetrahydrofuran and methylethylketone (90/10 in volume ratio).

Figure 4 shows the electron micrographs of ultrathin sections of film specimens of the TR-41-1649 block copolymer (as a reference) and of two blends of the block copolymer with 20% homopolystyrenes having average molecular weights of 4,800 and 20,400, respectively. The two blend systems also have alternating lamellar domain structures similar to that of the pure block copolymer. Since the molecular weights of the added homopolystyrenes are either lower than or comparable to those of the styrene segments in the block copolymer, they are well-solubilized (16)

into the styrene domains of the original block copolymer specimen shown in Fig. 4(a). Figs. 4(b) and 4(c) show that the solubilization has resulted in thickened PS domains.

Hereafter, the film specimens of the TR-41-1649 block copolymer and the blend of the block copolymer with the high molecular weight polystyrene are redesignated as "SBS" and "SBS/PS" specimens, respectively, and are mainly used for assuring the above postulation on the structural changes associated with the strain-softening and healing processes by means of electron microscopic and small angle X-ray scattering investigations.

The micrographs indicate that the original unstretched specimens of the SBS and SBS/PS have randomly oriented alternating lamellar microdomains of styrene and butadiene components. The blended homopolystyrene in the SBS/PS specimen is solubilized into the polystyrene lamellae, resulting in thickening of the PS lamellae. Stretching the SBS specimen by 85% elongation produces irregular deformation of the lamellar microdomains accompanied by shearing, kinking, disruption and orientation of the lamellar microdomains (Fig. 5a). These deformation processes are responsible for the yielding and necking of the specimen and are dominant until the necking is completed.

Upon further stretching, fragmentation of the lamellar microdomains prevails. Finally fragmented polystyrene domains are dispersed in the matrix of polybutadiene, as can be seen in Fig. 5(b). These fragmentation processes must have been responsible for the plastic-to-rubber transition. The polystyrene fragments act as surface-active filler particles for polybutadiene, and the elasticity of the specimen is essentially entropic in origin. Quantitative aspects of the deformation processes can best be analyzed by the small angle X-ray scattering (SAXS) experiments.

It is also observed in Fig. 5(c) that the fragmented polystyrene domains are transformed into the original lamellar domains after "resting"

in the unstretched state for several days at room temperature. The heat generated during the embedding and restaining processes, however, may have contributed to the reformation process also. The reformed structure is more perfect when it is annealed at elevated temperature, as seen in Fig. 5(d), and less perfect for the SBS/PS. The reappearance of lamellar morphology, however, is obvious in both types of healing process.

Small Angle X-ray Scattering

Figure 6 shows the logarithm of the desmeared relative intensity as a function of scattering angle (2θ in minutes). The unstretched SBS specimen (bottom curve) shows the first-order and the third-order scattering maxima at $2\theta = 19.7$ and 60 minutes, respectively. The second-order scattering maximum which is supposed to appear at $2\theta \simeq 40$ minutes is not clearly observed due to the fact that volume fractions of the two lamellae are nearly equal. This results in decreased intensity of the second-order scattering maximum (extinction rule) and overlapping tails of the first-order and the third-order maxima at this angle. Each scattering maximum corresponds to the first- and higher-order scattering maxima of a single lamellar spacing of 269 Å. The homopolystyrene which was blended into the SBS is solubilized, as shown in Fig. 4, so that the lamellar spacing of the unstretched SBS/PS specimen (upper curve) is increased to 319 Å, as indicated in the figure. Due to the blending, volume fraction of the polystyrene lamellae is now greater than 50%. The intensity of the second-order maximum increases and thereby becomes clearly discernible.

Figure 7 shows the change in SAXS patterns upon stretching the SBS specimen in the first stretch half-cycle. The figure also includes schematic representations of the SAXS patterns with only the first

scattering maxima. The numbers in the figure indicate percent elongations of the specimens. Upon stretching the meridional SAXS maxima tend to shift toward smaller angles. Its intensity decreases until 30% elongation where it disappears. This indicates that the lamellae, originally oriented with their boundaries normal to the stretch direction, increase their spacing with elongation. However, the spacing also becomes irregular due to such deformation processes as shearing, kinking, and destruction of the lamellae. The relation between the extension ratio in bulk to that of the lamellar spacing ($d_{//}/d_o$), estimated from the change of the first- and the third-order scattering maxima, is plotted in Fig. 8(a) for the initial stage of stretching (less than 30%-elongation). On the other hand, the equatorial SAXS maxima remain nearly invariant under the same conditions, as seen in the same figure for the d_1/d_o data, which indicates that the spacings do not vary for those lamellae which were originally oriented parallel to the stretch direction. This accounts for the volume dilatation of the specimen.

At higher elongations, the equatorial scattering maximum disappears due to the deformation processes discussed above. The scattering patterns in the pleateau region of the stress-strain curve after the yield-point are characteristic of lamellar surfaces inclined to the stretch direction, as schematically shown in Fig. 8(b). With increasing bulk extension ratio the scattering lobes tend to be elongated parallel to the equator, i.e., the lateral breadth of the lobe increases, indicating that the lamellae are fragmented so that their lateral continuity decreases. Moreover, the spacing parallel to the stretch direction (d) is seen to increase with extension ratio as the distance between scattering lobes in the stretch direction decreases with increasing bulk extension ratio. This is quantitatively demonstrated in the plot of

of $d_{//}/(d_{//})_{1.3}$ vs bulk extension ratio in Fig. 8(b), where $d_{//}$ is the spacing parallel to the stretching direction and $(d_{//})_{1.3}$ is that at the bulk extension of 1.3 at which the four-point pattern begins to develop. The spacing d in the direction perpendicular to the lamellar surfaces was also measured as a function of the bulk extension ratio, as indicated in fig. 8(b). Since $d = d_{//} \cos \alpha$, where α is the angle between the stretching direction and the lamellar normal, the fact that the spacing d hardly changes with the bulk extension ratio, in contrast to $d_{//}$, indicates that the lamellar surfaces tend to orient parallel to the stretching direction so that the angle α increases.

Upon further stretching, scattering lobes disappear. The scattering pattern becomes diffuse, and is more or less independent of the azimuthal angle. The implication is that fragmented polystyrene domains are randomly dispersed in the rubber matrix. This is consistent with the conclusion obtained by a qualitative examination of the electron micrographs in Fig. 5. The polystyrene domains now act as filler particles, on which surfaces the polybutadiene chains (the middle block segments of the SBS) must be anchored, and the sample exhibits rubber-like elasticity.

Figure 9 shows a schematic representation of the change of the SAXS patterns for the SBS (left) and SBS/PS (right) specimens. The general trend in the change of SAXS patterns for the SBS/PS specimen is identical to that for the SBS specimen. For the SBS/PS specimen, however, the structural regularity tends to be more easily destroyed, resulting in more extensive fragmentation than the SBS specimen.

Figure 10 summarizes schematically the structural changes occurring in the strain-induced plastic-to-rubber transition. The change in structure from (a) to (b) illustrates the initial stage of deformation of the microdomain up to the yield-point, as

observed in the expansion of the lamellar spacing for the lamellae oriented perpendicular to the stretching direction. The changes in structure from (b) to (d) illustrate the expected changes in the yielding and necking processes in which the irregular deformation of the lamellar microdomains occurs. The deformation involved kinking, shearing, destruction, and orientation of the lamellae. Finally, fragmented polystyrene domains are randomly dispersed in the rubber matrix, as illustrated in (e), and act as surface-active filler particles for the polybutadiene chains in the matrix.

To further examine the effect of healing on morphology, we show in Figure 11(a) and 11(b) the SAXS patterns of the SBS and SBS/PS samples released from 355%-elongation and rested at room temperature for a few days, and in Figs. 11(c) and 11(d) the patterns of the SBS and SBS/PS specimens released from 390%- and 500%-elongation, respectively, then both annealed at 59°C for 5 hr. In all figures the stretching direction is vertical. As can be seen in Figs. 11(a) and 11(b), no significant change in the SAXS patterns is observed upon healing, except for a faint reappearance of the first-order maximum at equatorial zone for the SBS specimen. Therefore, the structure becomes sufficiently regular to give the scattering maxima up to the third order. As expected the reformation process is slow at room temperature. On the other hand, Fig. 11(c) show that annealing at 59°C substantially restores the original lamellar domain structure, especially for the SBS specimen, though the lamellar spacing parallel to the stretching direction is still slightly expanded than that normal to it. It is of interest to note that structural reformation does occur at a temperature as low as 59°C, which is considerably lower than the glass-transition temperature of polystyrene.

Figures 12 and 13 show electron micrographs of ultrathin sections of the SBS and SBS/PS specimens, respectively. Both display the healing effect after releasing from 500%-elongation (the stretching direction is horizontal). Here (a) is after healing at room temperature for a few days and (b), (c) and (d) show the healing effect followed by annealing at 60,88, and 116°C, respectively, all for 5 hr. Although the initial stretching of the specimens up to 500%-elongation is larger than that for the SAXS test in Fig. 11, the structural reformation is generally much more pronounced for the SBS specimen than for SBS/PS, and its general trend is consistent with that expected from SAXS patterns shown in Fig. 11. For example, in Fig. 12(a) the reformed domain structure is still largely oriented in the stretch direction with less regular lamellar spacing parallel to the stretch direction than that perpendicular to it, giving rise to the SAXS pattern shown in Fig. 11(a). The electron micrograph of Fig. 5(c) more closely resembles that of Fig. 12(b) than 12(a), suggesting that heat generated during the embedding and restaining processes has a non-negligible effect on the observed structure.

Figs. 14(a) and 14(b) show the changes of equatorial SAXS intensity distribution around the first-order maximum for various durations of healing at room temperature and at an elevated temperature of 60°C. The SAXS intensity distributions from unstretched (original) and stretched (500%-elongation) specimens are also included for comparison. These figures demonstrate the recovery of the diffuse SAXS intensity distribution of the stretched specimen to relatively sharp first-order maximum of the original specimen. At room temperature no significant recovery can be seen up to 4 hr., while at 60°C almost complete recovery, except for a slight shift of the maximum to higher scattering angles, can be obtained in a duration as short as 10 minutes.

When the duration is longer than 10 min., the first-order maximum becomes more intensive and closer in peak position to that of the original specimen, suggesting not only the recovery of the domain structure in lamellar spacing but also the increased regularity of lamellar structure, i.e., the annealing effect.

Dynamic Mechanical Properties

Figure 15 shows the temperature dispersion of isochronal complex dynamic tensile modulus functions at a fixed frequency of 10 Hz for the SBS/PS specimen in unstretched and stretched (330%-elongation) states. The two temperature dispersions around -100 and 90°C in the unstretched state may be assigned to the primary glass transitions of the polybutadiene and polystyrene domains. In the stretched state, however, these loss peaks are broadened and shifted to around -80 and 80°C respectively. In addition, new dispersion peak appears at around 40°C. The shift of the primary dispersion of polystyrene domain toward lower temperatures and the appearance of an additional dispersion may be attributed to the fragmentation of the polystyrene lamellar domains.

The existence of an additional dispersion has been noted by several authors for the heterogeneous systems of block and graft co-polymers and been assigned to a type of grain-boundary phenomena (17,18). It has however, not always been found in other studies (19-24). The existence of the interfacial domain-boundary has also been investigated theoretically (13,14,15) and experimentally from SAXS intensity distribution in terms of the domain-boundary thickness (25,26,27). Fragmentation of the polystyrene lamellae due to stretching must greatly increase the specific surface area of the styrene phase, and therefore the volume fraction of the interfacial domain-boundary region, (27), resulting in the opposite shift of the primary

dispersion of the polystyrene domain, as suggested by Bares (28), as well as the appearance of the additional dispersion.

The fact that the structural reformation of the original lamellar domains from the fragmented ones can occur even at a temperature as low as 60°C and a duration as short as 10 min., as demonstrated in Fig. 14(b), may be explained in terms of (A) cancellation of free energy increase in the system associated with orientation of the polybutadiene chains, (B) enormous increases of the specific surfaces in the system and (C) the enhanced volume fraction of the interfacial domain-boundary region. In this region, the polystyrene segments must be intermixed with polybutadiene segments, so that the polystyrene chains may gain enough mobility required for the structural reformation even under conditions as mild as annealing at 60°C for 10 min.

Acknowledgements

The authors are indebted to the Shell Development Co. for supplying the tri-block copolymers TR-41-1647, TR-41-1648 and TR-41-1649. H. Kawai and M. Shen also wish to thank the Japan Society for the Promotion of Science, the Dreyfus Foundation and the Office of Naval Research for support which has enabled them to cooperate in their research projects on hetro-phase systems including this paper.

Literature Cited

1. Beecher, J.F., Marker, L., Bradford, R.S., Aggarwal, S.L., J. Polymer Sci. (1969), C26, 117.
2. Henderson, J.F., Grundy, K.F., Fischer, E., J. Polymer Sci. (1968), C16, 3121.
3. Fischer. E., Henderson, J.F., J. Polymer Sci., (1969), C26, 149.

4. Akovali, G., Niinomi, M., Diamant, J., Shen, M., ACS Polymer Preprints, (1976), 17, 560.

5. Hong, S.D., Shen, M., Russell,T., Stein, R.S., in "Polymer Alloys," D. Klempner and K.C. Frisch, eds., Plenum, New York, 1977.

6. Hendus, H., Illers, K.H., Ropte, E., Kolloid-Z.u.Z. Polymere, (1967), 216, 110.

7. Fischer, E., J. Macromol. Sci.-Chem., (1968), A2, 1285.

8. Toy, L., Niinomi, M., Shen, M., J. Macromol. Sci.-Phys., (1975), B11, 281.

9. Hendricks, R.W., Schmidt, P.W., Acta Physica Austriaca, (1973), 37, 20.

10. Schmidt, P.W., Acta Cryst., (1965), 19, 938.

11. Todo, A., Fujimura, M., Hashimoto, T., Kawai, H., J. Appl. Cryst., in press.

12. Inoue, T., Soen, T. Hashimoto, T., Kawai, H., J. Polymer Sci., (1969), A-2, 7, 1283.

13. Leary, D.J., Williams, M.C., J. Polymer Sci., (1970), B, 8, 335.

14. Meier, D.J., ACS Polymer Preprints, (1974), 15, 171.

15. Helfand, E., Accounts of Chemical Research, (1975), 8, 295.

16. Inoue, T., Soen, T., Hashimoto, T., Kawai, H., Macromolecules, (1970), 3, 87.

17. Saito, N., Okano, K., Iwayanagi, S., Hideshima, T., in "Solid State Physics," H. Ehrenreich, F. Seitz, and D. Turnbull Eds., Vol. 14, Academic Press, New York, 1963, p. 458.

18. Aggarwal, S.L., Livigni, R.A., Marker, L.F., Dudek, T.J., in "Block and Graft Copolymers," J.J. Burke and V. Weiss Eds., Syracuse University Press, Syracuse, N.Y., 1973.

19. Shen, M., Kaelble, D., J. Polymer Sci., (1970), B8, 149.

20. Fesko, D.G., Tschoegl, N.W., Intern. J. Polymeric Mater., (1974), 3, 51.

21. Soen, T., Ono, T., Yamashita, K., Kawai, H., Kolloid-Z.u.Z. Polymere, (1972), 250, 459.

22. Soen, T., Shimomura, M., Uchida, T., Kawai, H., Colloid & Polymer Sci., (1974), 252, 933.

23. Kraus, G., Rollmann, K.W., J. Polymer Sci., Polymer Phys. Ed., (1976), 14, 1133.

24. Akovali, G., Diamant, J., Shen, M., J. Macromol, Sci.-Phys., (1977), B13, 117.

25. Hashimoto, T., Nagatoshi, K., Todo, A., Hasegawa, H., Kawai, H., Macromolecules, (1974), 7, 364.

26. Hashimoto, T., Todo, A., Itoi, H., Kawai, H., Macromolecules, (1977), 10, 377.

27. Todo, A., Uno, H. Miyoshi, K., Hashimoto, T., Kawai, H., Polymer Eng. and Sci., (1977), 17, 587.

28. Bares, J., Macromolecules, (1975), 8, 244.

Captions for Figures

Fig. 1. Cyclic tensile stress-strain behavior of the spin-cast specimens, TR-41-1647, TR-41-1648, and TR-41-1649, at 25°C at a constant rate of tensile strain, 50%/min. The tensile stress is expressed in terms of true stress. The specimens were air-dried without heating.

Fig. 2. Cyclic tensile stress-strain behavior of TR-41-1649 and its blend with polystyrene ($\bar{M}$: 20,400) at room temperature at a constant rate of tensile strain, 50%/min. The curves (1) and (2) refer to the first and second stretching half cycles, respectively,

and the tensile stress is expressed in terms of nominal stress.

Fig. 3. Electron micrographs of ultrathin sections of film specimens spin-cast from 10% solutions of a series of tri-block copolymers; (a) TR-41-1647, (b) TR-41-1648 and (c) TR-41-1649, all in a mixture of tetrahydrofuran and methyl ethyl ketone in volume ratio of 90/10, and stained by OsO_4.

Fig. 4. Electron micrographs of ultrathin sections of film specimens spin-cast from 10% solutions of; (a) TR-1649 alone, (b) mixture of TR-41-1649 with homopolystyrene ($\bar{M}$: 4,800) in weight ratio of 80/20, and (c) mixture of TR-41-1649 with homopolystyrene ($\bar{M}$: 20,400) in weight ratio of 80/20, all in a mixture of tetrahydrofuran and methylethylketone in volume ratio of 90/10, and stained by OsO_4.

Fig. 5. Electron micrographs of ultrathin sections of SBS film specimens; (a) stretched to 80%, (b) stretched to 500% (c) released from 600% and left unstretched at room temperature for several days, and (d) released from 600%-elongation and heat-treated at 100°C for 2 hrs. The sectioning was made parallel to the stretching direction and normal to the film surfaces. The stretching direction is horizontal.

Fig. 6. Logarithms of relative desmeared intensity distributions of SAXS from the SBS-PS (upper curve) and SBS (bottom curve) specimens plotted against scattering angles 2θ in minutes.

Fig. 7. Change in SAXS patterns of the SBS specimen during the course of the first stretch half-cycle. The stretch direction is vertical.

Fig. 8. The relation between the extension ratio in bulk and that of the spacing; (a) at the initial stage of stretching (less than 30%-elongation) and (b) at large elongations.

Fig. 9. Schematic representation of changes in SAXS patterns for the SBS (left) and SBS/PS (right) specimens during the first and second stretching half-cycles.

Fig. 10. Schematic representation of the deformation processes involved in the strain-induced plastic-to-rubber transition.

Fig. 11. SAXS patterns of the SBS and SBS/PS specimens taken during the healing process at room temperature and at an elevated temperature; (a) SBS specimen released from 355%-elongation and left in unstretched state at room temperature for a few days. (b) SBS/PS specimen released from 355% elongation and left in unstretched state at room temperature for a few days, (c) SBS specimen released from 390%-elongation and annealed at 59°C for 5 hr., and (d) SBS/PS specimen released from 500%-elongation and annealed at 59°C for 5 hr.

Fig. 12. Electron micrographs of ultrathin sections of the SBS specimens released from 500%-elongation and (a) left in unstretched state at room temperature for a few days, and annealed at (b) 60°C, (c) 88°C, and (d) 116°C for 5 hr. Sectioning was made parallel to the stretching direction and normal to the film surfaces. The stretch direction is horizontal.

Fig. 13. Electron micrographs of ultrathin sections of the SBS/PS specimens released from 500%-elongation and (a) left at

room temperature for a few days, and (b), (c) and (d) annealed at 60, 88, and 116°C, respectively, all for 5 hr. The sectioning and stretching directions are the same as those in Fig. 12.

Fig. 14. Healing effect of the SBS specimen released from 500%-elongation, investigated from the change of SAXS intensity distribution around the first-order scattering maximum with duration of staying; (a) at room temperature and (b) at 60°C.

Fig. 15. Temperature dispersion of isochronal complex dynamic tensile modulus function at a fixed frequency of 10 Hz, observed for the SBS/PS specimen at unstretched and stretched (330%-elongation) states.

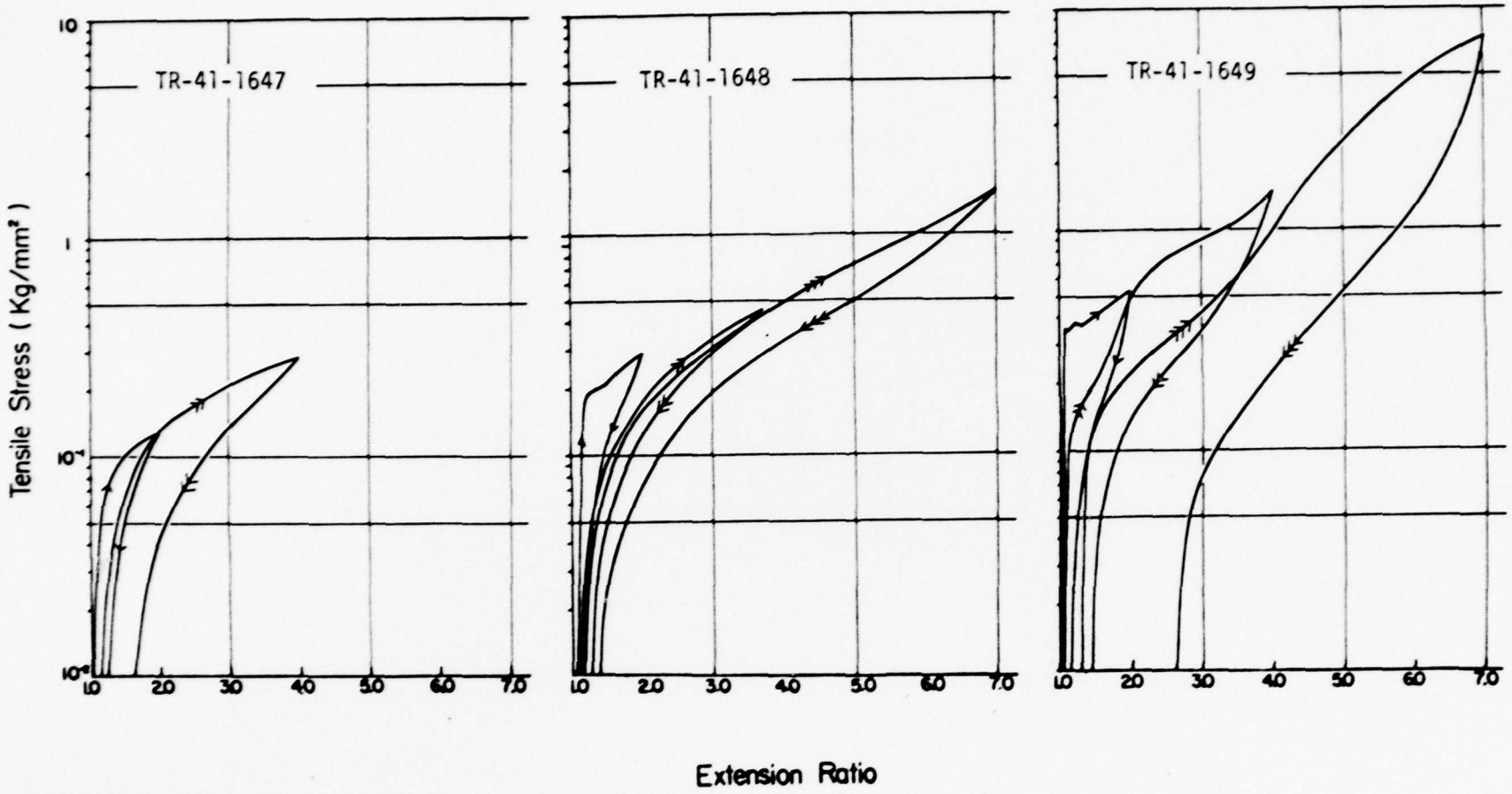
TR-41-1647
TR-41-1648
TR-41-1649
Tensile Stress (Kg/mm²)
10
1
10⁻¹
10⁻²
1.0
2.0
3.0
4.0
5.0
6.0
7.0
Extension Ratio

Fig. 1.

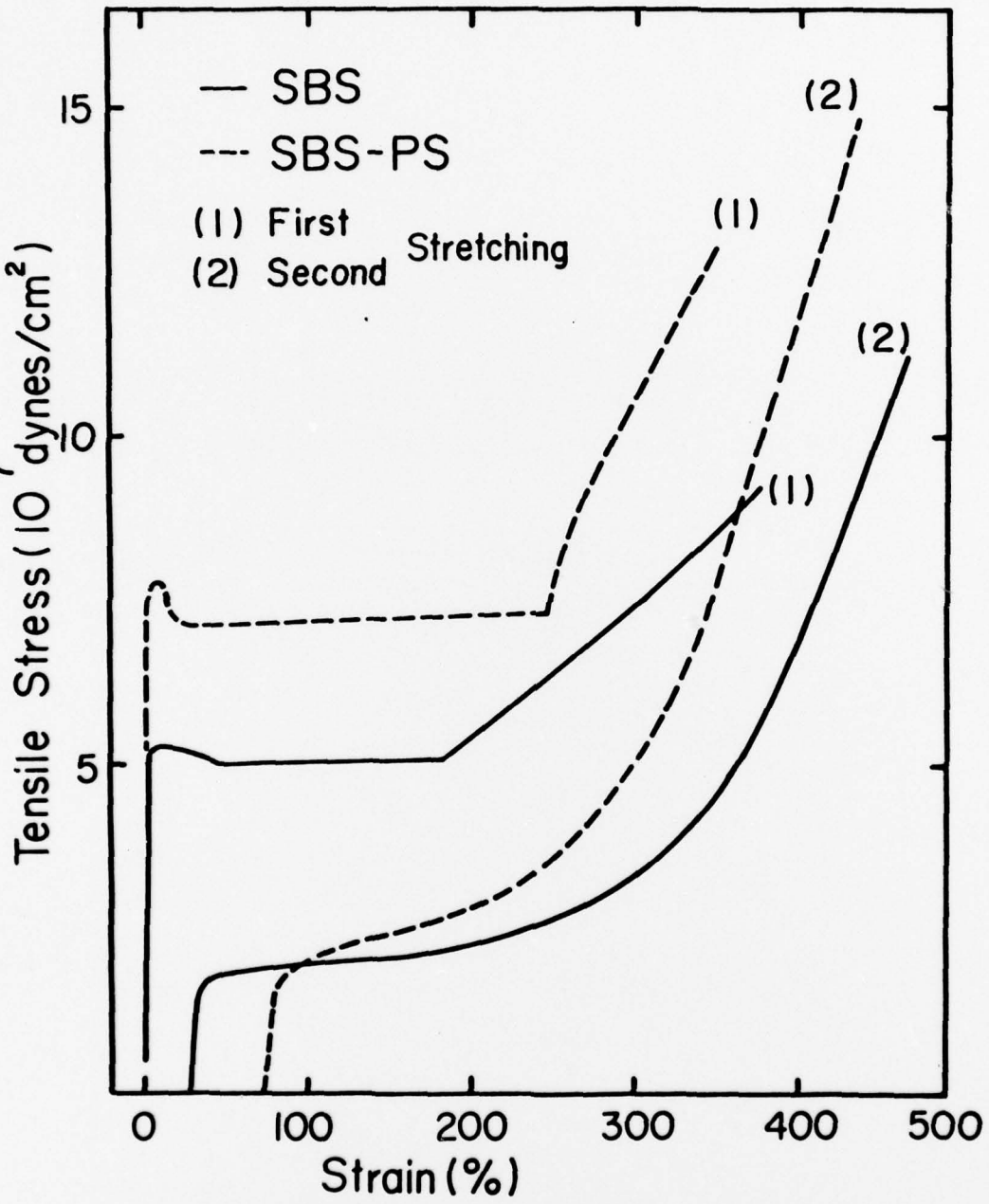
— SBS
--- SBS-PS
(1) First
(2) Second Stretching
(1)
(2)
(2)
(1)
15
10
5
Tensile Stress (10^7 dynes/cm^2)
0
100
200
300
400
500
Strain (%)

Fig. 2.

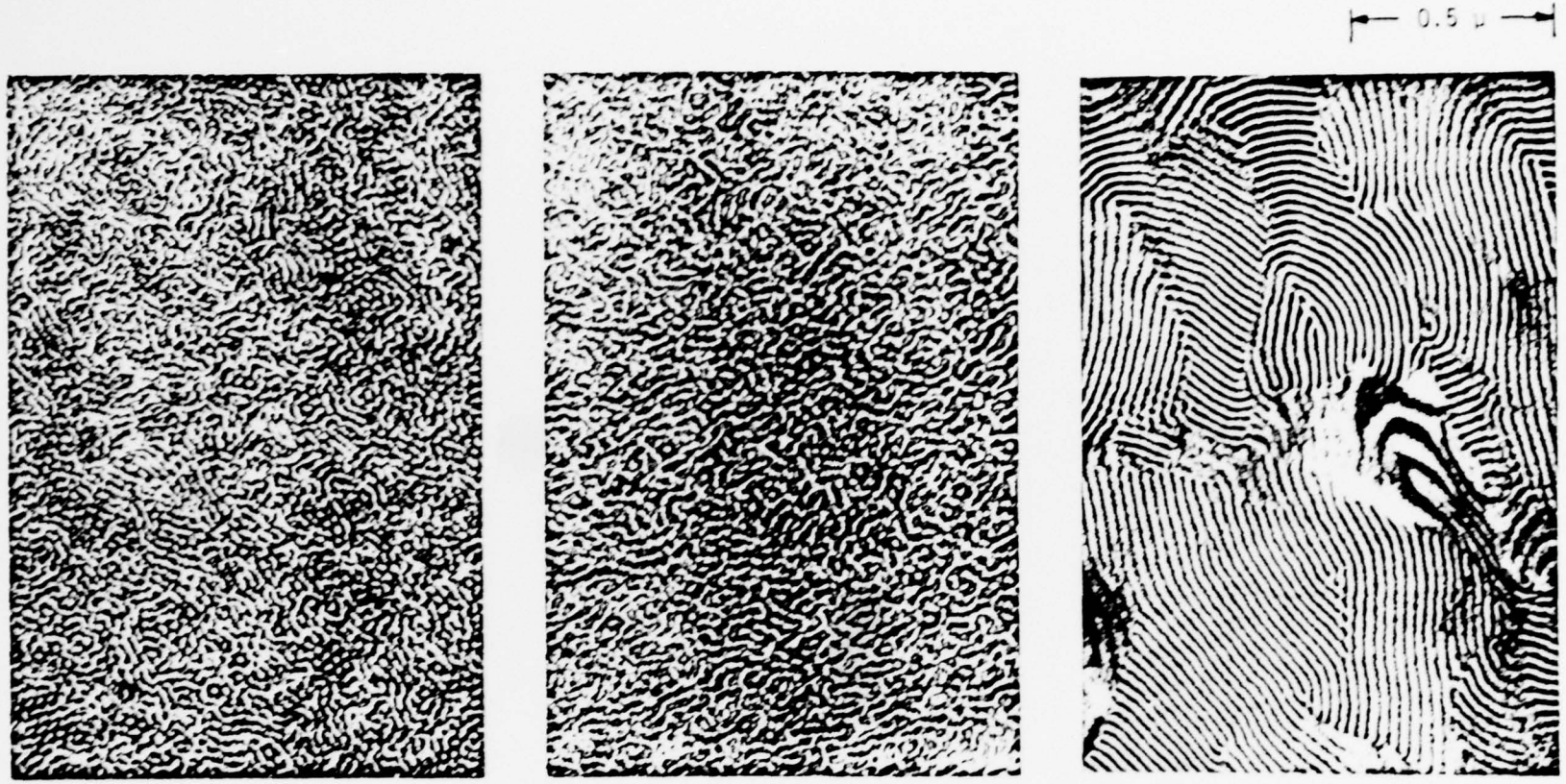

Fig. 3.

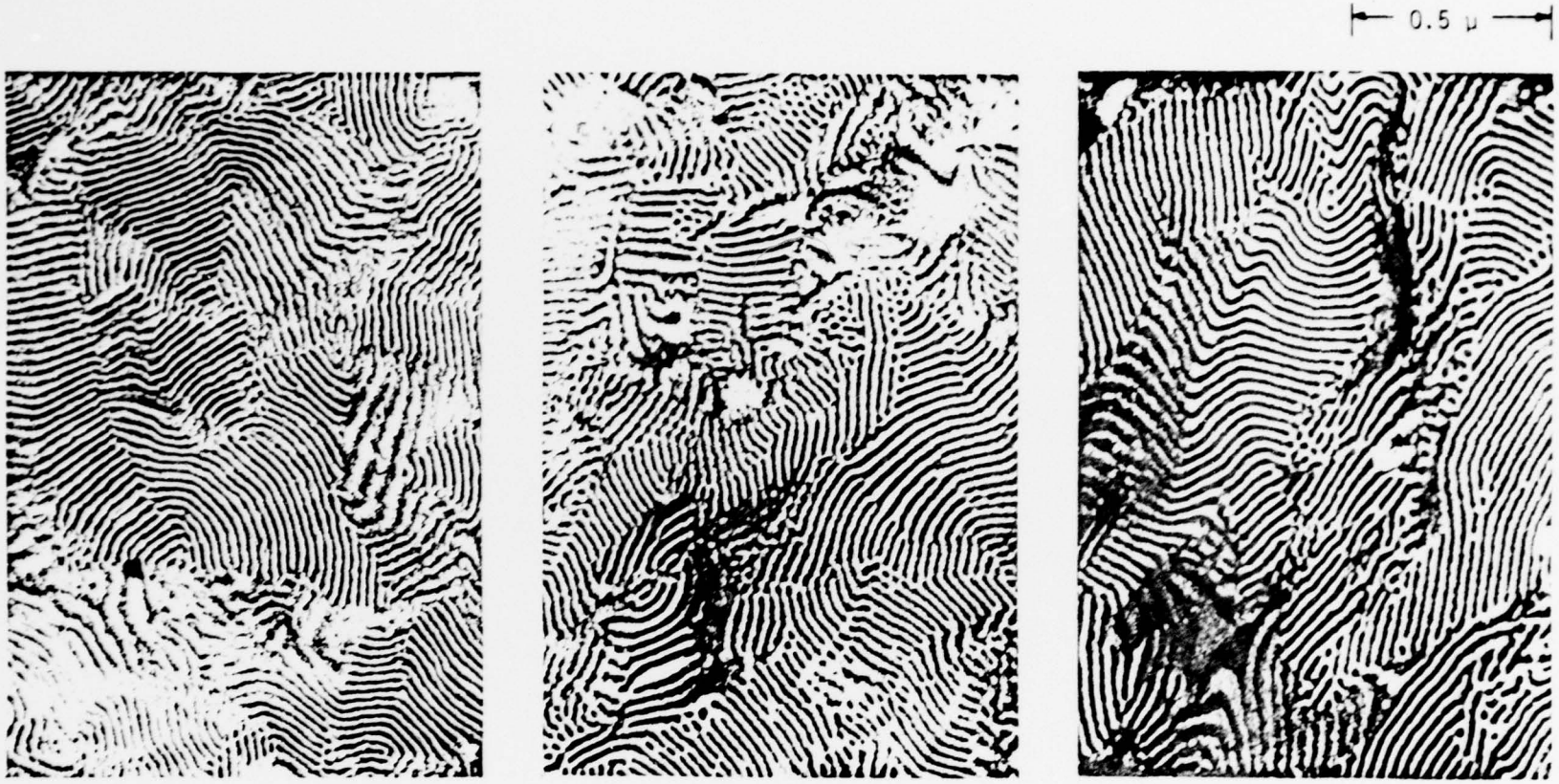

Fig. 4.

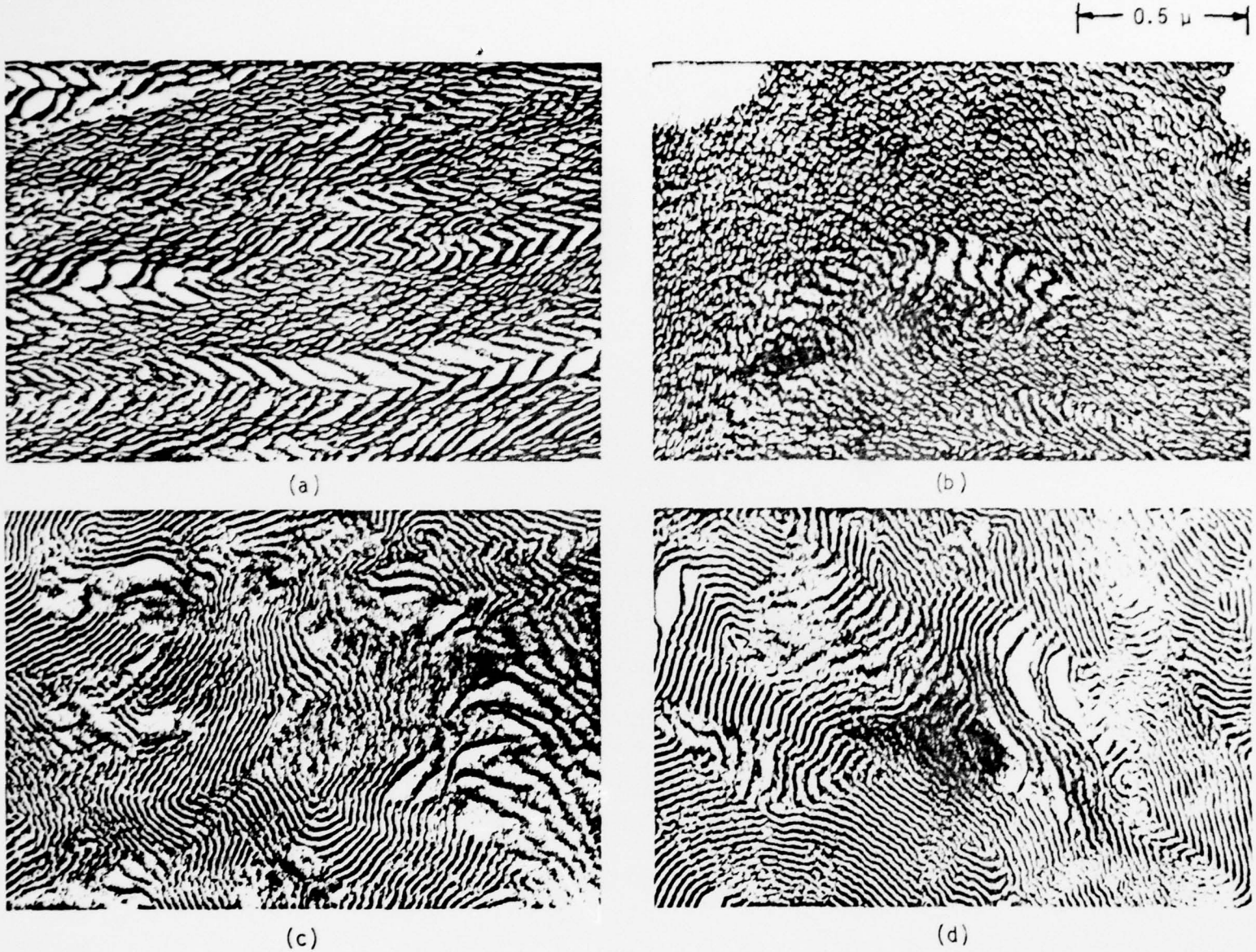

Fig. 5.

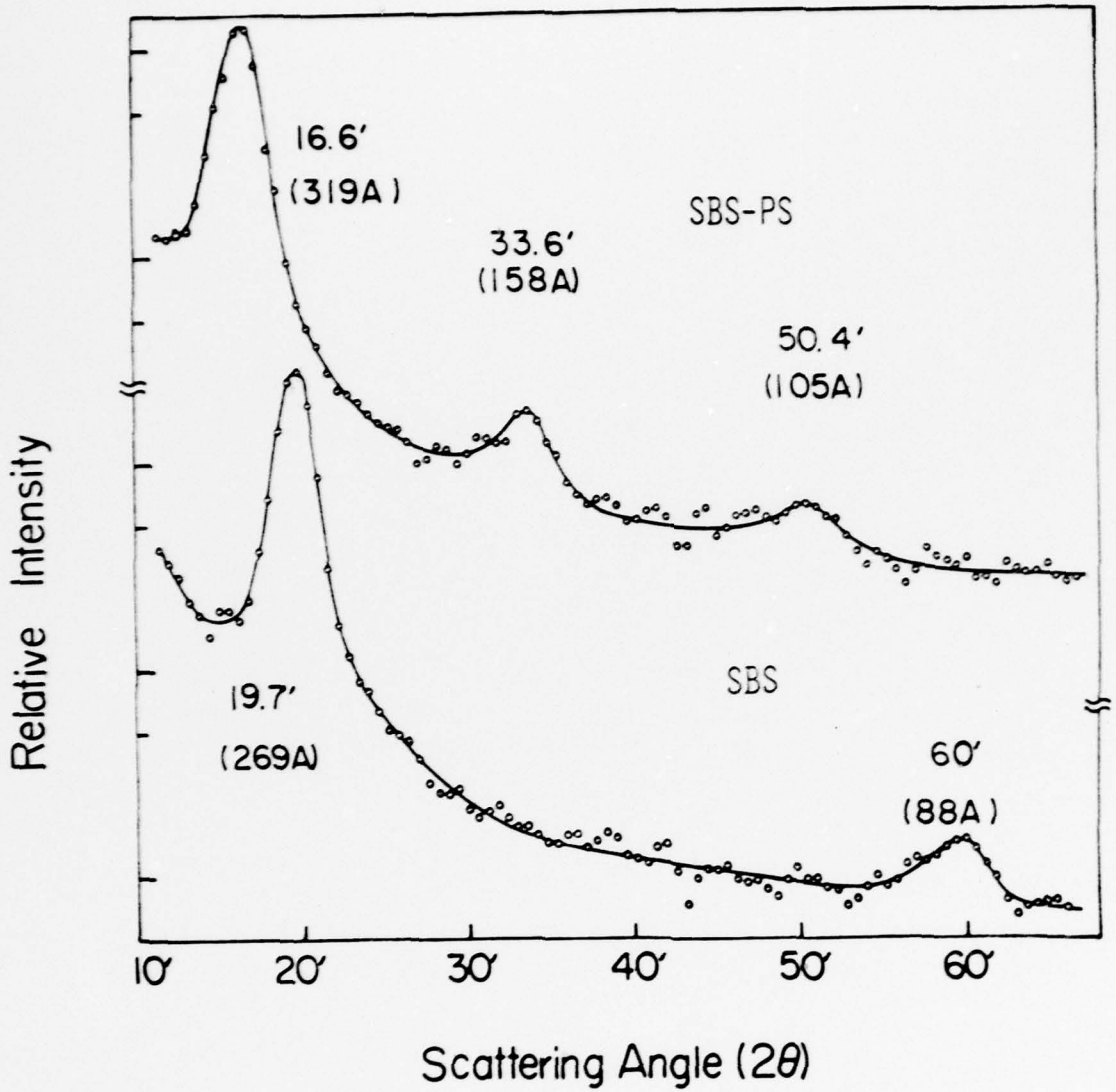
16.6'
(319A)
SBS-PS
33.6'
(158A)
50.4'
(105A)
19.7'
(269A)
SBS
60'
(88A)
Relative Intensity
10'
20'
30'
40'
50'
60'
Scattering Angle (2θ)

Fig. 6.

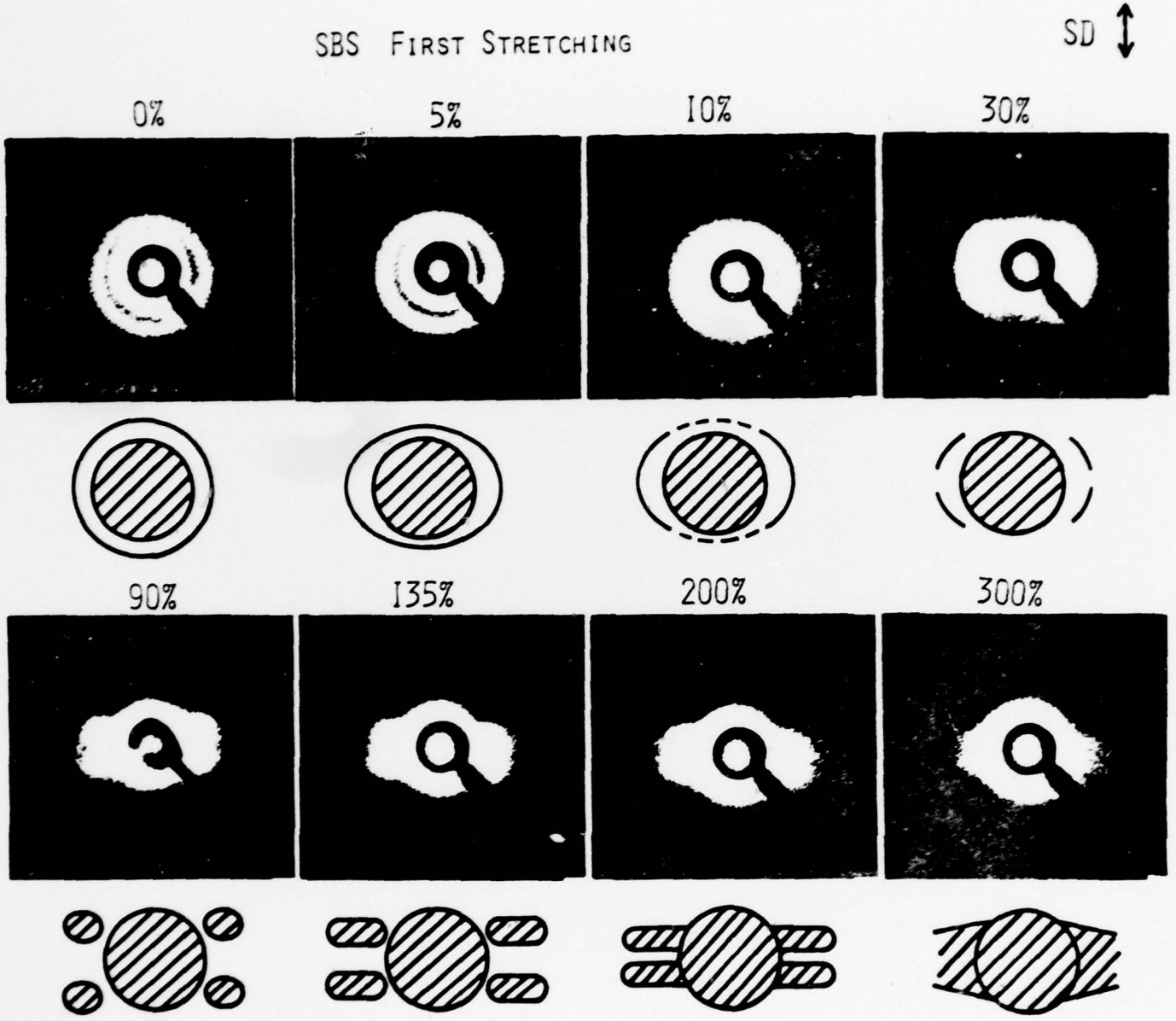

Fig. 7.

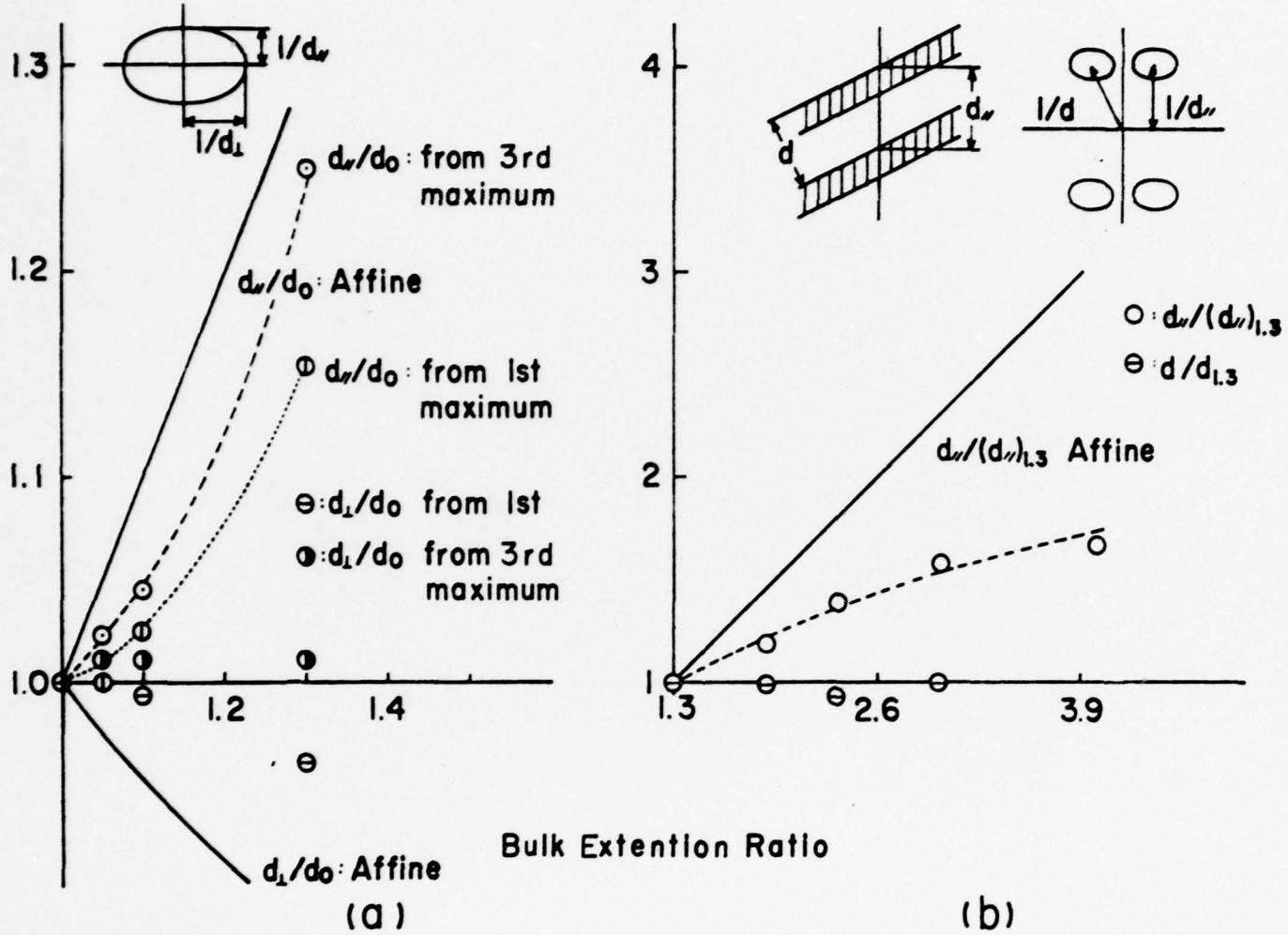
1.3
1.2
1.1
1.0
1.2
1.4
$1/d_{//}$
$1/d_{\perp}$
$d_{//}/d_0$: from 3rd maximum
$d_{//}/d_0$: Affine
$d_{//}/d_0$: from 1st maximum
$d_{\perp}/d_0$ from 1st
$d_{\perp}/d_0$ from 3rd maximum
$d_{\perp}/d_0$: Affine
(a)
4
3
2
1
1.3
2.6
3.9
$d_{//}$
d
1/d
$1/d_{//}$
$d_{//}/(d_{//})_{1.3}$
$d/d_{1.3}$
$d_{//}/(d_{//})_{1.3}$ Affine
Bulk Extention Ratio
(b)

Fig. 8.

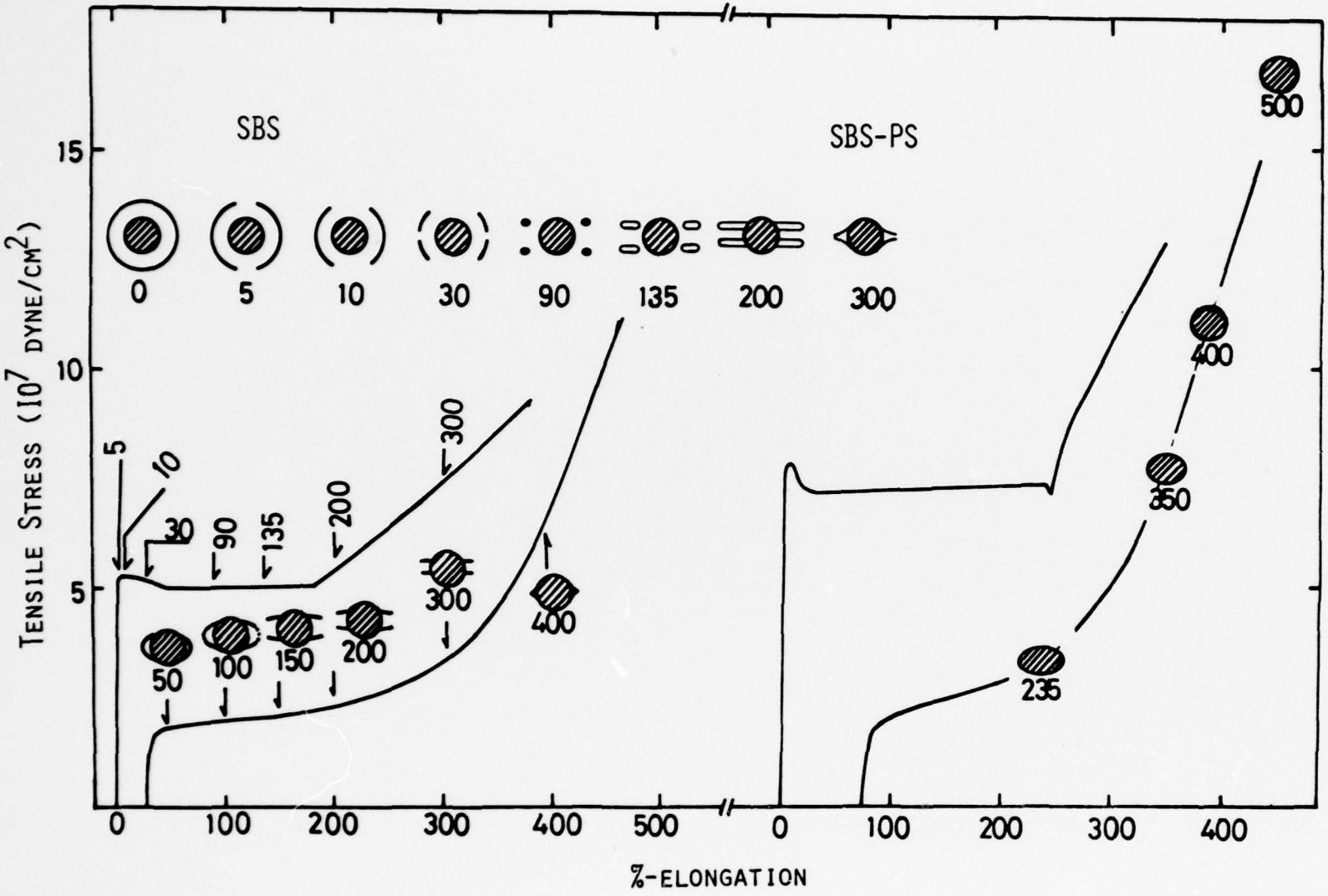
SBS
SBS-PS
0
5
10
30
90
135
200
300
500
400
350
235
50
100
150
200
300
400
TENSILE STRESS (10^7 DYNE/CM^2)
%-ELONGATION
0
100
200
300
400
500
5
10
15

Fig. 9.

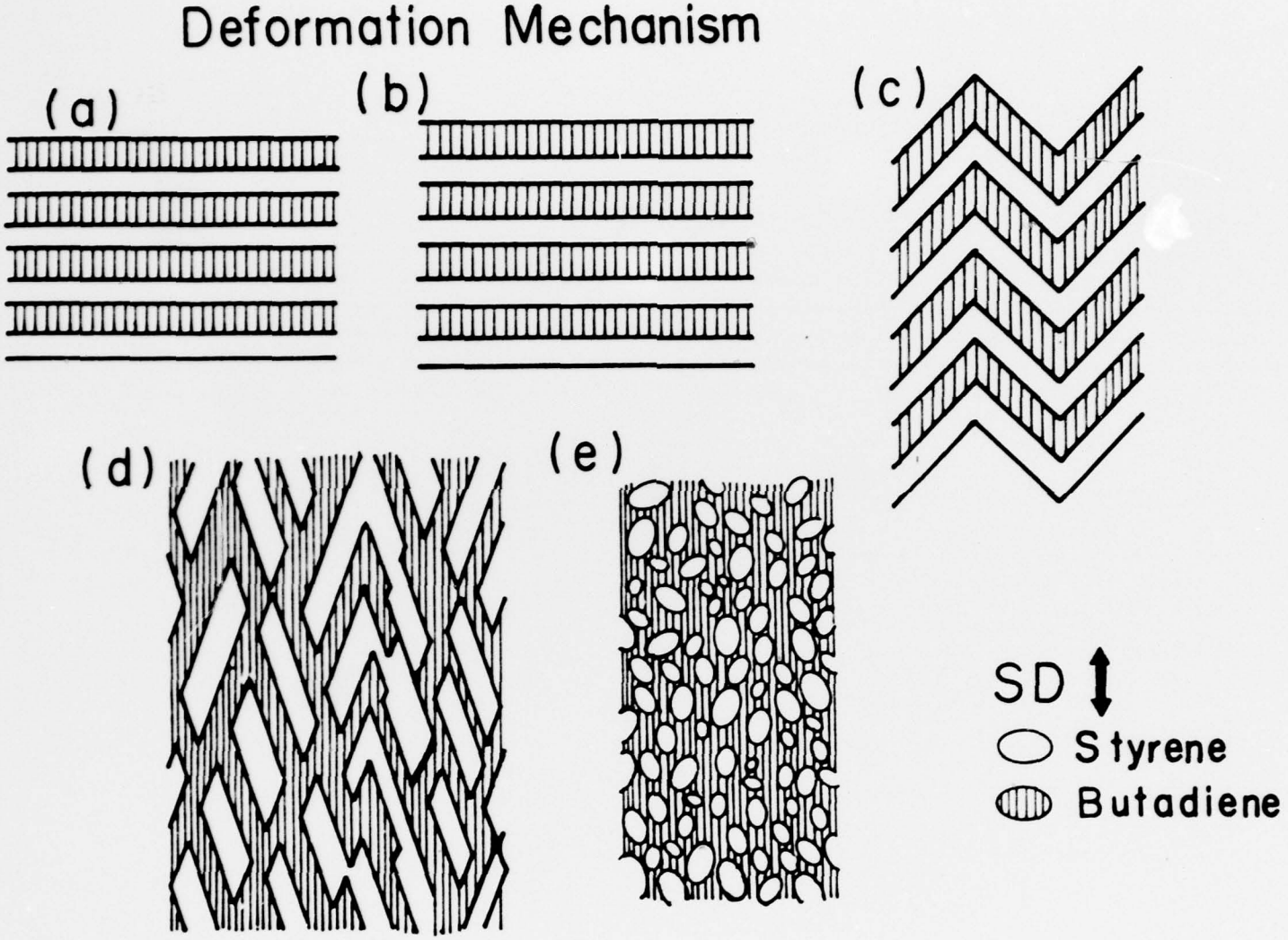

Fig. 10.

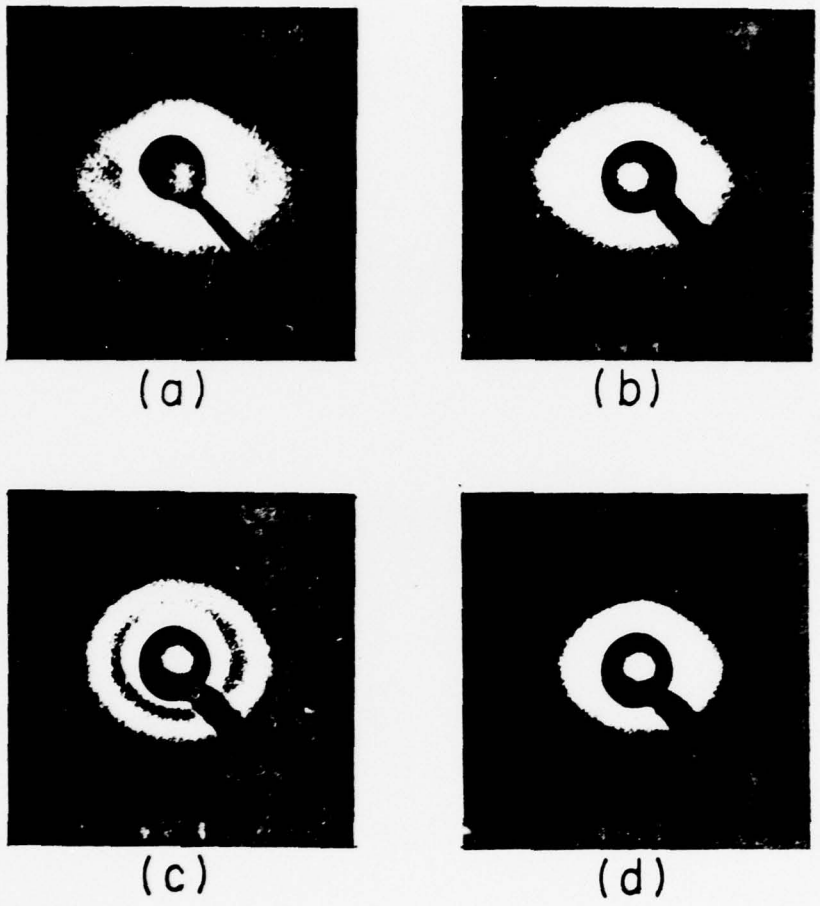

Fig. 11.

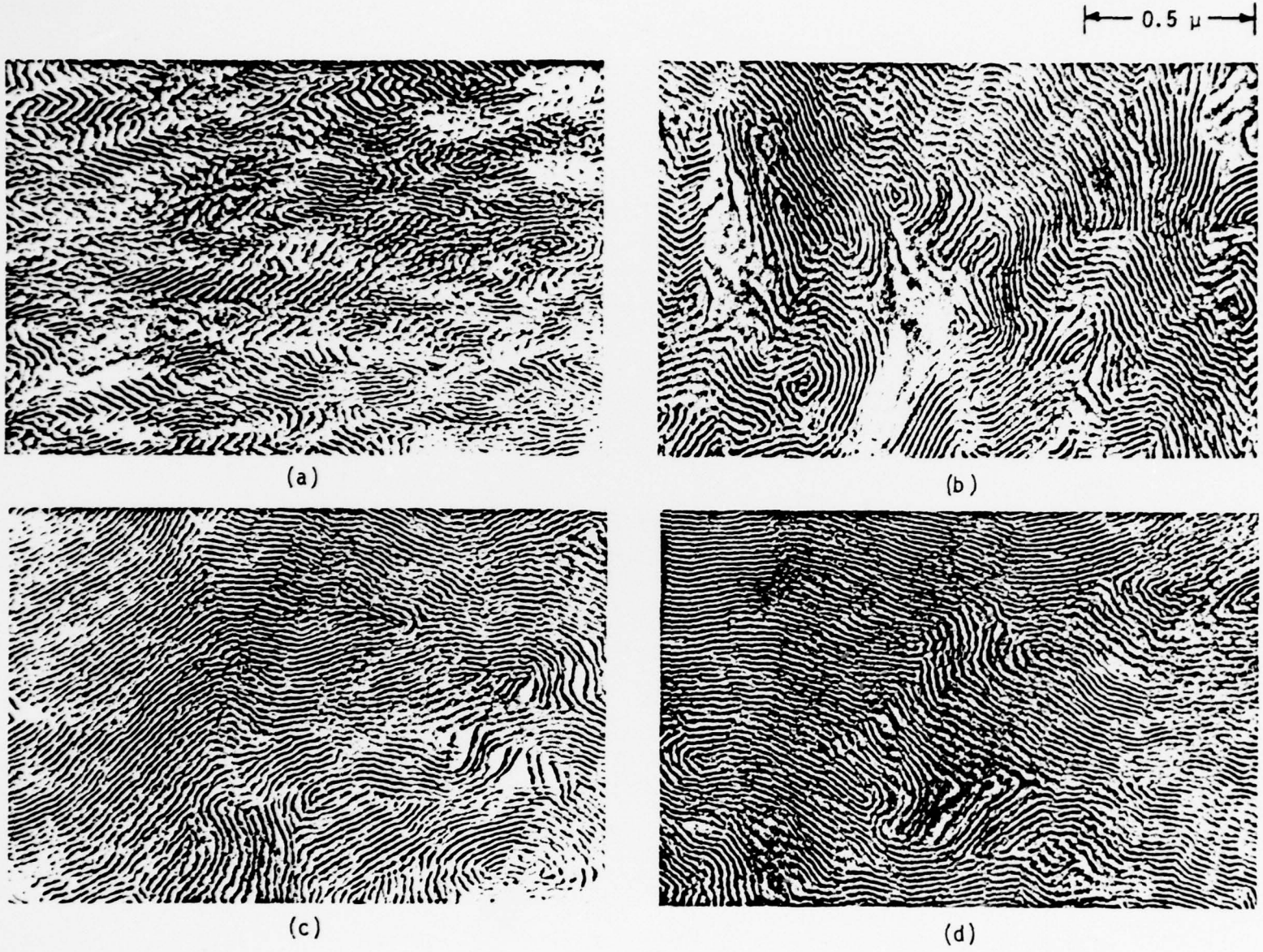

Fig. 12.

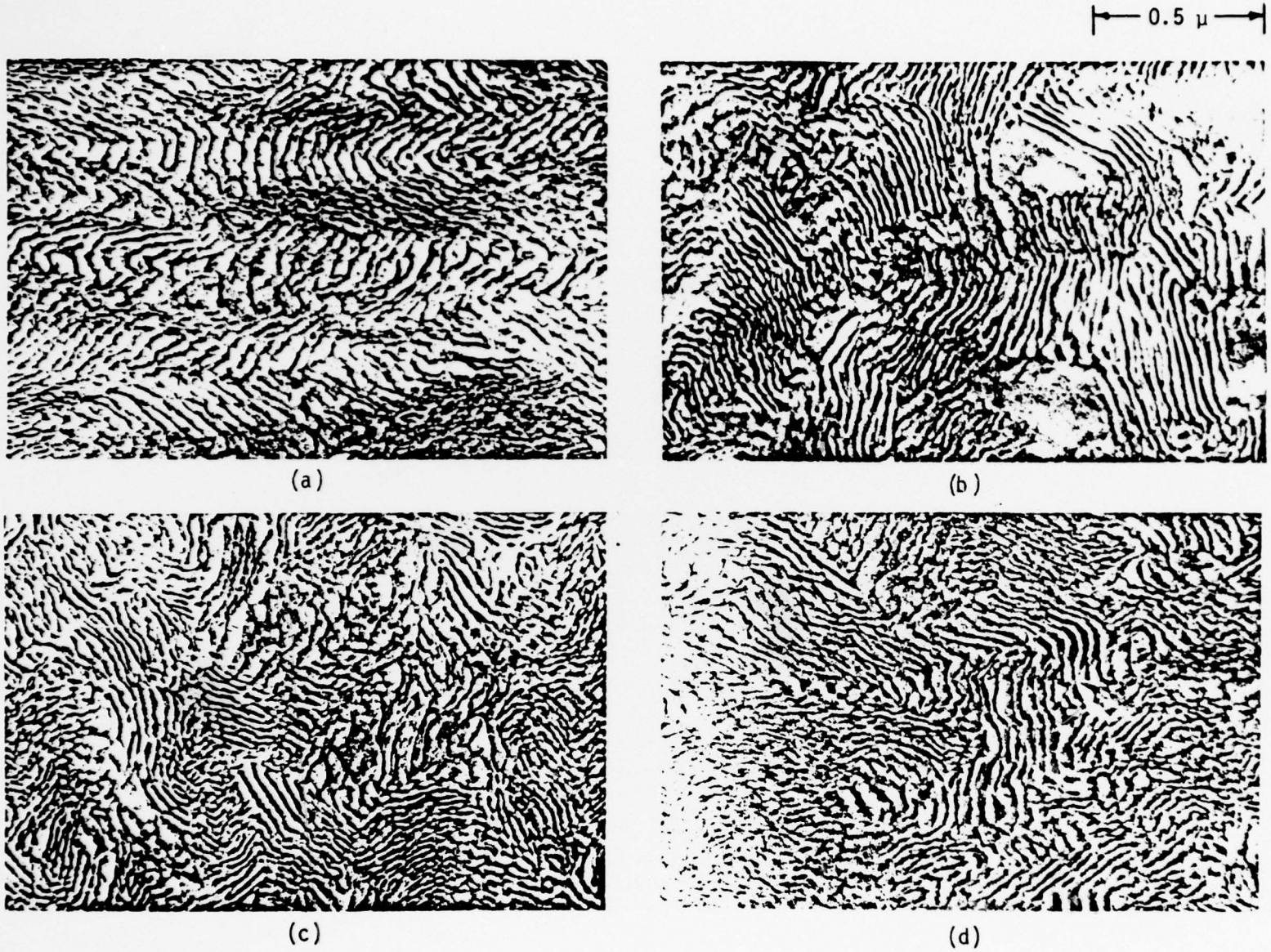

Fig. 13.

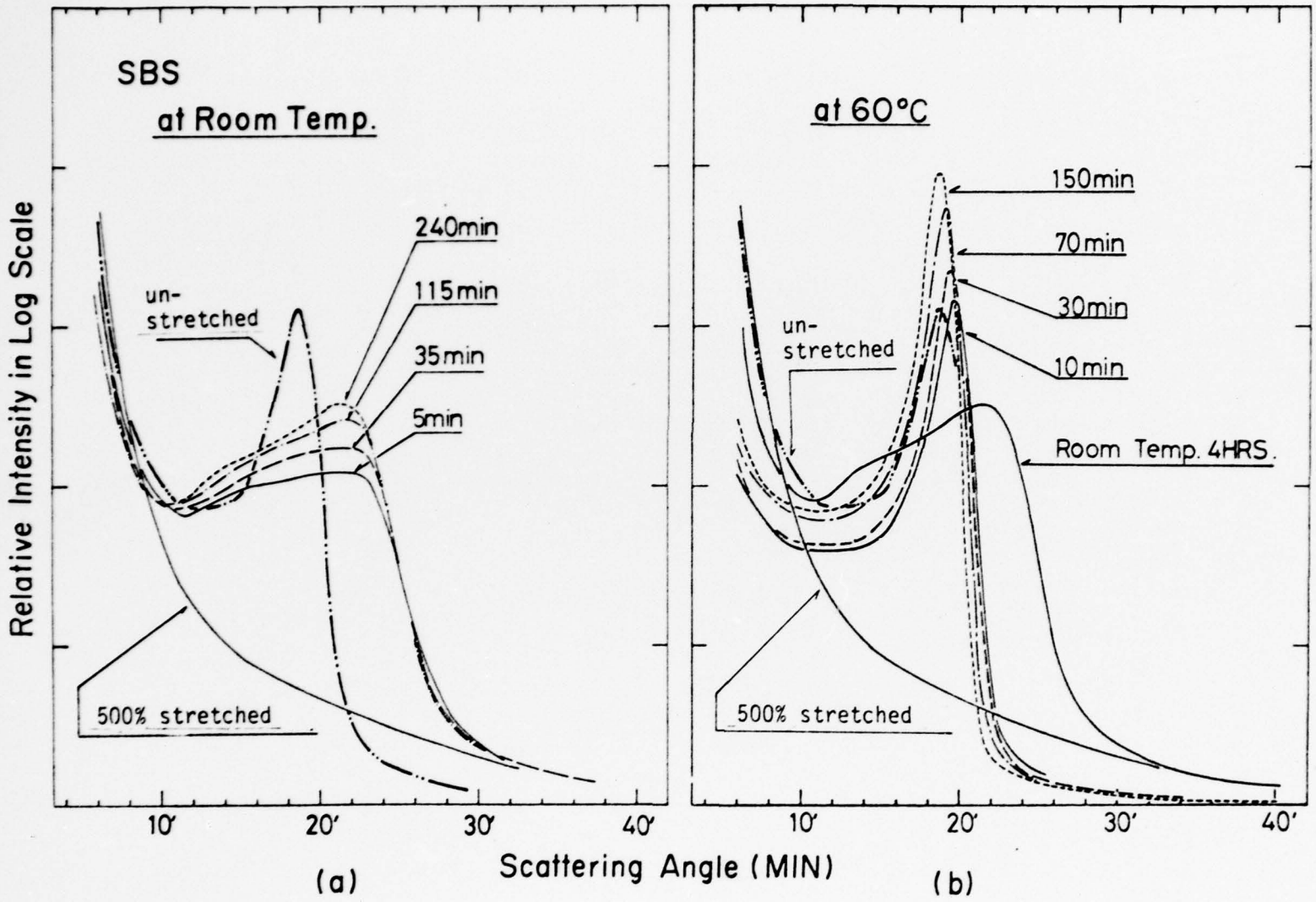
SBS
at Room Temp.
240min
115min
35min
5min
un-
stretched
500% stretched
at 60°C
150min
70min
30min
10min
un-
stretched
Room Temp. 4HRS.
500% stretched
Relative Intensity in Log Scale
10'
20'
30'
40'
Scattering Angle (MIN)
(a)
(b)

Fig. 14.

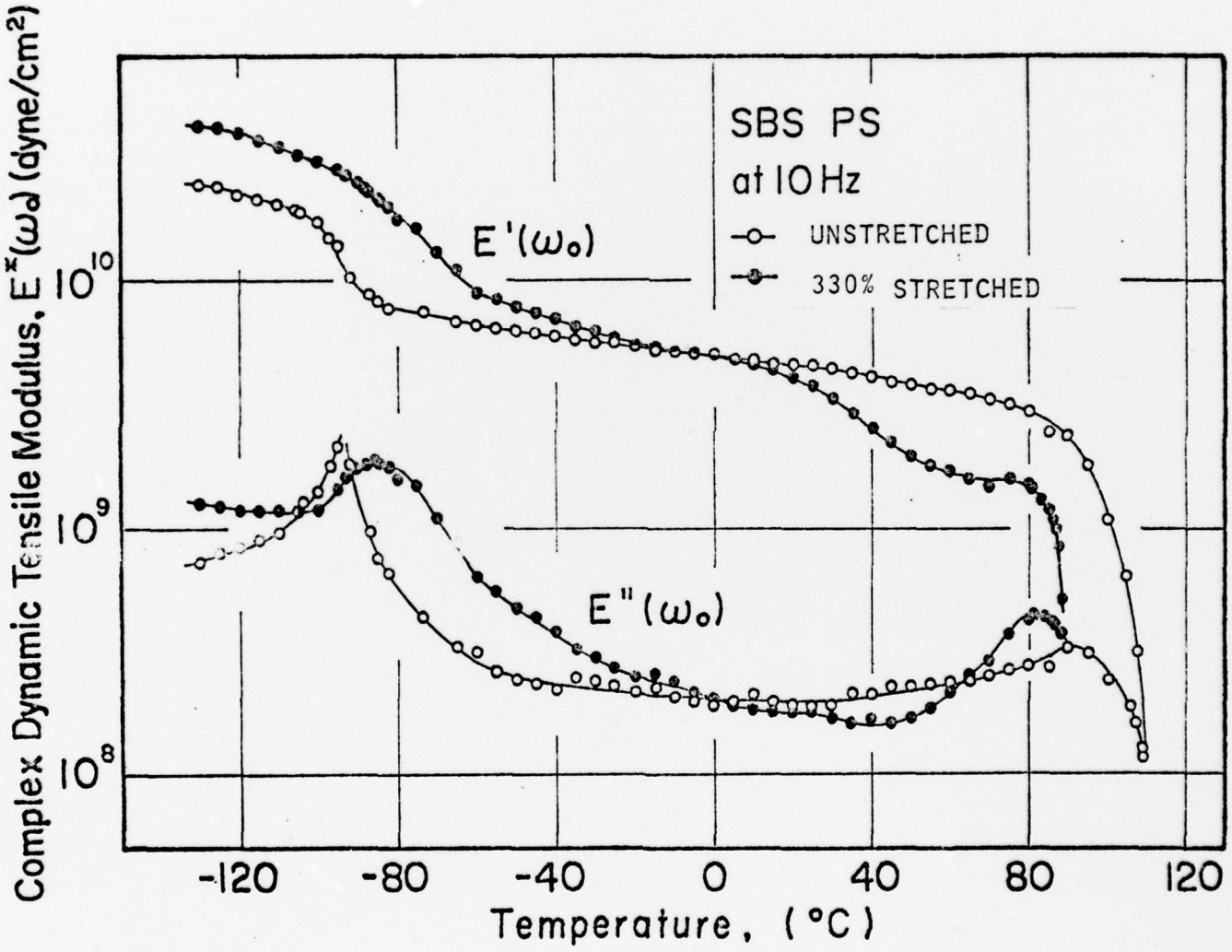
SBS PS
at 10 Hz
UNSTRETCHED
330% STRETCHED
E'(ω₀)
E"(ω₀)
Complex Dynamic Tensile Modulus, E*(ω₀) (dyne/cm²)
10¹⁰
10⁹
10⁸
-120
-80
-40
0
40
80
120
Temperature, (°C)

Fig. 15.